Available online at www.sciencedirect.com

ScienceDirect

Procedia Structural Integrity 21 (2019) 206–214

Structural Integrity Procedia

www.elsevier.com/locate/procedia

1st International Workshop on Plasticity, Damage and Fracture of Engineering Materials

Simulation of Drop-Weight Impact Test on Composite Laminates using Finite Element Method

Mirac Onur Bozkurt[a,b], Levend Parnas[c], Demirkan Coker[a,b,*]

[a]*Department of Aerospace Engineering, METU, Ankara 06800, Turkey*
[b]*METU Center for Wind Energy, METU, Ankara 06800, Turkey*
[c]*Department of Mechanical Engineering, TED University, Ankara 06800, Turkey*

Abstract

This study presents the simulation of standard drop-weight impact test on a $[0/90/0]_s$ composite laminate. For this purpose, a three-dimensional virtual test setup is developed in ABAQUS/Explicit finite element tool. Hemispherical impactor and specimen fixture are modeled as rigid bodies. Composite plate is modeled as a 3-D deformable solid and discretized using a biased mesh for computational efficiency. For simulation of ply damage in the composite laminate, a continuum damage mechanics based damage model is developed and implemented into the analysis via a user-written subroutine VUMAT. Delamination damage is simulated by inserting cohesive elements at the interfaces of plies having different orientations. Results show that the initial failure mechanism in the 3-D low-velocity impact event is the matrix cracking in the lowermost plies independent from the stacking sequence of the laminate. Furthermore, the simulation accurately predict that delaminated regions expand mainly in the same direction as of the fibers of the lower adjacent layer in accordance with the bending stiffness mismatching concept.

Peer-review under responsibility of the 1st International Workshop on Plasticity, Damage and Fracture of Engineering Materials organizers

Keywords: Drop-weight impact; finite element analysis; composite; matrix crack; delamination

* Corresponding author. Tel.: +90-312-210-4257; fax: +90-312-210-4250.
E-mail address: coker@metu.edu.tr

Peer-review under responsibility of the 1st International Workshop on Plasticity, Damage and Fracture of Engineering Materials organizers
10.1016/j.prostr.2019.12.103

1. Introduction

Use of fiber-reinforced plastics (FRP) in engineering applications is favorable because they offer numerous advantages such as light weight, high stiffness and strength. However, laminated FRP composites are susceptible to delamination damage which leads to considerable losses in the residual strength. In the design phase, damage tolerance analysis consisting of sequential transverse impact and compression after impact (CAI) analyses are conducted with certified methods. Since testing alone is highly expensive due to the manufacturing and testing of large number of coupons required to verify every geometry, loading, environment and failure mode, development of virtual test setups which accurately predicts impact damage and CAI strength is of great interest.

In the literature, several studies are conducted on developing virtual impact test setups. Lopes et al. (2009) investigated the effect of dispersed stacking sequences on impact response of fiber-reinforced polymers by use of constitutive models which take into account the physical progressive failure behaviour of fibres, matrix, and interfaces between plies. Later, Gonzalez et al. (2012) conducted simulations of sequential impact and compression-after-impact tests using finite element method. Topac et al. (2017) simulated their line impact experiments on $[0/90]_s$ beams by implementing the constitutive material models into the finite element model and predict damage formation process in agreement with their experiments. More recently, Soto et al. (2018) simulated low velocity impact and compression after impact in large composite stiffened panels using continuum damage mechanics based material models.

In this study, a virtual drop-weight impact test setup is developed to simulate standard large mass - low velocity impact tests (ASTM, 2012). 3D finite element model is generated in ABAQUS/Explicit. Hemispherical impactor and specimen fixture are modeled as rigid bodies. 3D solid elements are used in modeling of the cross-ply composite laminate. Constitutive material model accounts for both interlaminar and intralaminar failure modes and it is implemented via a user-written VUMAT subroutine. Damage formation process is investigated in detail. In order to assess the accuracy of the simulations, comparisons with experimental results are performed.

2. Modelling of low-velocity impact damage

Two distinct material model is used for simulation of low-velocity impact damage in composite laminates: (i) a continuum damage mechanics based material model accounting for ply level damage modes including fiber and matrix failure, (ii) a cohesive damage model for simulation of delamination.

2.1. Intralaminar damage model

A continuum damage mechanics based intralaminar damage model predicting initiation and evolution of composite damage is developed with 3-D stress formulation. The model accounts for fiber and matrix damages in tension and compression modes.

Damage initiation in tensile fiber (FT), compressive fiber (FC), tensile matrix (MT) and compressive matrix (MC) modes are controlled by failure indexes FI_N. When the FI_N reaches unity, damage in corresponding mode initiates. Maximum stress and Hashin Failure Criteria (Hashin, 1980) are used for longitudinal and transverse failure indexes, respectively, which are given for each damage mode as

$$FI_{FT} = \frac{\sigma_{11}}{X_T} \tag{1}$$

$$FI_{FC} = -\frac{\sigma_{11}}{X_C} \tag{2}$$

$$FI_{MT} = \left(\frac{\sigma_{22} + \sigma_{33}}{Y_T} \right)^2 + \frac{\sigma_{23}^2 + \sigma_{22}\sigma_{33}}{S_{23}^2} + \left(\frac{\sigma_{12}}{S_{12}} \right)^2 + \left(\frac{\sigma_{13}}{S_{13}} \right)^2 \tag{3}$$

$$FI_{MC} = \left[\left(\frac{Y_C}{2S_{23}} \right)^2 - 1 \right] \frac{\sigma_{22} + \sigma_{33}}{Y_C} + \left(\frac{\sigma_{22} + \sigma_{33}}{2S_{23}} \right)^2 + \frac{\sigma_{23}^2 - \sigma_{22}\sigma_{33}}{S_{23}^2} + \left(\frac{\sigma_{12}}{S_{12}} \right)^2 + \left(\frac{\sigma_{13}}{S_{13}} \right)^2 \tag{4}$$

In equations (1) – (4), X_T and X_C are the longitudinal tensile and compressive, Y_T and Y_C are the transverse tensile and compressive strengths, S_{12}, S_{13} and S_{23} are the in-plane longitudinal, out-of-plane longitudinal and transverse shear strengths of a unidirectional ply.

The evolution of the damage is modelled by a linear softening response with equivalent stress-strain approach shown in Fig. 1a. The area under the curve corresponds to the energy dissipated per unit volume and is defined as

$$g_N = G_c^N / L^* \tag{5}$$

where L^* is the characteristic length of finite element and G_C^N is the fracture toughness for the damage mode N. The damage variable d_N shows a non-linear saturation type behavior, as expressed in Eq. (6), to provide the linear softening response of damaged material.

$$d_N = \frac{\varepsilon_{eq}^f \left(\varepsilon_{eq}^{max} - \varepsilon_{eq}^0 \right)}{\varepsilon_{eq}^{max} \left(\varepsilon_{eq}^f - \varepsilon_{eq}^0 \right)} \tag{6}$$

where ε_{eq}^0 and ε_{eq}^f are the equivalent strains at the initiation of damage and complete failure, respectively. The maximum value of equivalent strain, in time history, ε_{eq}^{max}, is used to satisfy the irreversibility of the existent damage.

2.2. Interlaminar Damage Model

The interlaminar damage model used in the analysis to simulate delamination damage is the one offered by ABAQUS finite element package (Simulia, 2012). Fracture mechanics based bilinear traction-separation response, seen in Fig. 1b, is assigned to each cohesive element. Since delamination is usually caused by multi-axial stress state subjecting to the interface, mode-mixity is taken account when modeling the cohesive material response.

The initial response of the cohesive element is assumed to be linear until a damage initiation where the slope of the line is called penalty stiffness, K_i *(i = I,II,III)*. The value of the penalty stiffness must be high enough to prevent interpenetration of the crack faces and to prevent artificial compliance from being introduced into the model by the cohesive elements. Initiation of interlaminar damage is controlled by quadratic nominal stress criterion which is given as

$$\left(\frac{T_I}{T_{o,I}} \right)^2 + \left(\frac{T_{II}}{T_{o,II}} \right)^2 + \left(\frac{T_{III}}{T_{o,III}} \right)^2 = 1 \tag{7}$$

In this equation, T_i and $T_{o,i}$ *(i=I,II,II)* are the tractions applying to the surface and interlaminar strengths for corresponding fracture modes, respectively. Once interlaminar damage initiates, Benzeggagh-Kenane criterion, given in equation (8), is used for modeling mixed-mode propagation of damage (Benzeggagh and Kenane, 1996).

$$G_c = G_{Ic} + (G_{IIc} + G_{IIIc} - G_{Ic})\left(\frac{G_{II} + G_{III}}{G_I + G_{II} + G_{III}}\right)^{\eta} \tag{8}$$

where G_I and G_{Ic} are the work done by tractions and the components of the fracture toughness in mode i fracture, respectively. η is the mode interaction parameter. Linear softening response is defined to the cohesive elements in the plane where damage initiation occurs. The cohesive damage variable d shows a non-linear saturation type behavior, as expressed in equation (9), to provide the linear softening response of damaged cohesive elements.

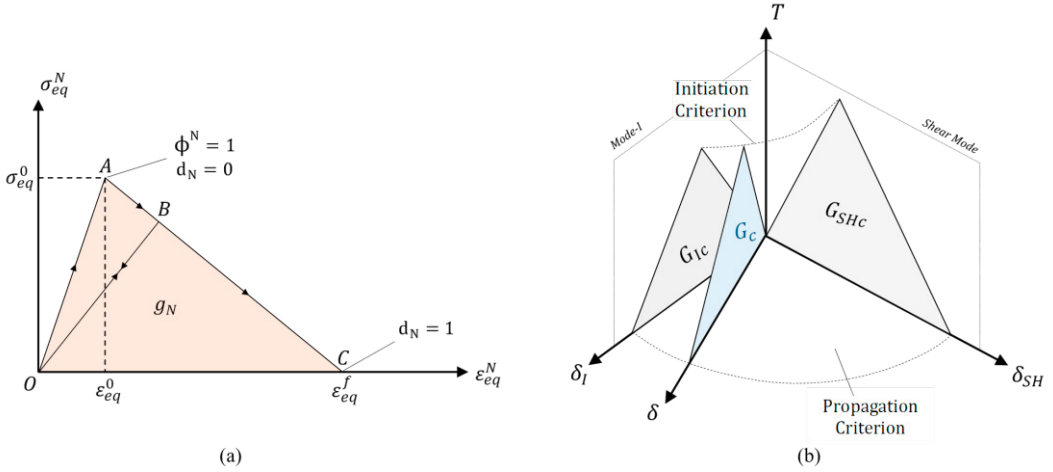

Fig. 1. (a) Linear softening response of ply material with equivalent stress-strain approach, (b) Mixed-mode bilinear traction-separation of cohesive material.

$$d = \frac{\delta_{eq}^{f}\left(\delta_{eq}^{max} - \delta_{eq}^{0}\right)}{\delta_{eq}^{max}\left(\delta_{eq}^{f} - \delta_{eq}^{0}\right)} \tag{9}$$

where $\delta_{eq}{}^{0}$, $\delta_{eq}{}^{f}$ are the equivalent displacements at the initiation of damage and complete failure, respectively, while $\delta_{eq}{}^{max}$ is the maximum value of equivalent displacement in time history.

3. Virtual test setup

To simulate low-velocity impact experiments on composite plates, three-dimensional finite element model is generated in ABAQUS/Explicit. The model consists of a 3-D deformable composite plate of 150×100 mm^2, a rigid fixture base having a 125×75 mm^2 window, four rigid cylindrical clamps with 10 mm diameter and a rigid semi-spherical impactor with 16 mm diameter. The assembly of the virtual test setup consisting of these parts is shown in Fig. 2.

$[0_4/90_4/0_2]_s$ composite plate of which the geometry is shown in Fig. 2 is modeled as a three dimensional deformable solid body. The plate consists of 20 unidirectional composite layers having equal thicknesses of 0.125 mm. In the model, clustered plies are considered as a single homogenized thick ply. Plate geometry is meshed with 8-noded linear brick elements with reduced integration and hourglass control (C3D8R in ABAQUS library). Each two ply of composite beam is modeled with one element in through-the-thickness direction. In-plane mesh size is set variable to reduce the computational cost. A central region of 50×50 mm^2 including the impact zone is meshed uniformly with elements of 0.25×0.25×0.25 mm^3. A biased mesh is used outside of this region such that each element has a 1.1 times greater element size than the previous one while going towards plate boundaries. Material model accounting initiation and propagation of composite ply damage is defined to the finite elements in the central zone while only elastic

behavior is found adequate for the remaining elements. In order to prevent unrealistic element deformations due to numerical issues, enhanced hourglass control is introduced to the finite elements of the plate. Additionally, distortion of the elements is limited to the 10% of the original size for preventing excessive distortion due to the issues like negative element volume or material degradation. Cohesive regions are modeled at interfaces of plies with different orientations inside the central region and are composed of 0.25×0.25 mm^2 cohesive elements with zero thickness.

Carbon/epoxy material of which the mechanical and interface properties are given in Table 1 and Table 2 is used as the ply material of composite beam in the analysis. Most of the material properties are provided by the material supplier and measured using standard test methods. Only G_{I+}, G_{I-}, and η values are taken from Lopes et al. (2009) since the elastic and strength properties of the materials are similar.

Table 1. Mechanical properties of carbon/epoxy material.

Density	1520 kg/m^3
Elastic	E_1 = 140 GPa; E_2 = 9 GPa; E_3 = 9 GPa
	ν_{12} = 0.35; ν_{13} = 0.35; ν_{23} = 0.48
	G_{12} = 5 GPa; G_{13} = 5 GPa; G_{23} = 4 GPa
Strength	X_T = 2000 MPa; X_C = 1500 MPa
	Y_T = 65 MPa; Y_C = 220 MPa
	S_{12} = 110 MPa; S_{13} = 110 MPa; S_{23} = 83 MPa;
Toughness	G_{1+} = 81500 N/m ; G_{1-} = 106300 N/m
	G_{2+} = 270 N/m; G_6 = 570 N/m

Table 2. Interface properties of carbon/epoxy material.

Interface strength	$T_{o,I}$ = 65 MPa; $T_{o,II} = T_{o,III}$ = 110 MPa
Fracture toughness	$G_{I,c}$ = 270 N/m; $G_{II,c}$ = 570 N/m
B-K criterion constant	η = 1.45
Penalty stiffness	K_I = 3.6 x 10^{14} N/m^3; $K_{II} = K_{III}$ = 4.9 x 10^{14} N/m^3

Fixture base, which is a rectangular steel part having a rectangular window of 125×75 mm^2, is modeled as a discrete rigid body using with outer dimensions seen in Fig. 2. A total of 1220 Quadratic rigid elements (R3D4 in ABAQUS library) are used for discretization of the fixture base. All degrees of freedoms of the reference point associated with the fixture base are constrained in accordance with the standard experiment. In the assembly, the composite plate is located on the fixture base. Four discrete rigid clamps are positioned on the top surface of the plate at the start of the simulation, as seen in Fig. 2. Rigid clamps are also discretized using quadratic rigid elements (R3D4).

Hemi-spherical steel impactor is modeled as a discrete rigid body with 16 mm diameter and 3.387 kg mass. The discretization of the hemi-spherical impactor is made by spherified cube method and quadratic rigid elements (R3D4) are used. An initial velocity of 2.976 m/s corresponding to a 15 J impact is given to the impactor and it is located above the center of the composite plate. All degree of freedoms of the impactor except translation in vertical direction are restricted.

In the model, different contact interactions are defined between mating parts using general contact algorithm of the ABAQUS/Explicit: (i) between the impactor and top surface of the plate, (ii) between the bottom surface of the plate and top surface of the fixture base, (iii) between the clamp tips and the top surface of the plate, and (iv) inside the beam. The reason why a contact is defined inside the beam is opposing free surfaces form at the interfaces following a delamination damage. In all cases, hard contact with separation allowance is defined for interactions in normal direction. For tangential motion, contact is defined with Coulomb friction model with friction coefficients 0.3 and 0.5 for metal-to-composite and composite-to-composite contacts, respectively. Rough contact is defined between the rubber clamp tip and the composite plate meaning that no relative tangential motion occurs between these parts.

The analysis consists of two consequent solution steps. In the first step, with the aim of squeezing the plate between the fixture base and the clamps, rigid clamps are moved 0.005 mm downward with a smooth step during 0.0001 s. The resultant reaction force in each clamp is measured about 2700 N which is more than twice of the minimum clamping force specified in ASTM D7136 standard (2012). During the second solution step of the analysis, clamps are held stationary and the impactor moves downward with constant velocity until the initial contact between the impactor and the plate occurs. Analysis of the impact event is performed following the initial contact.

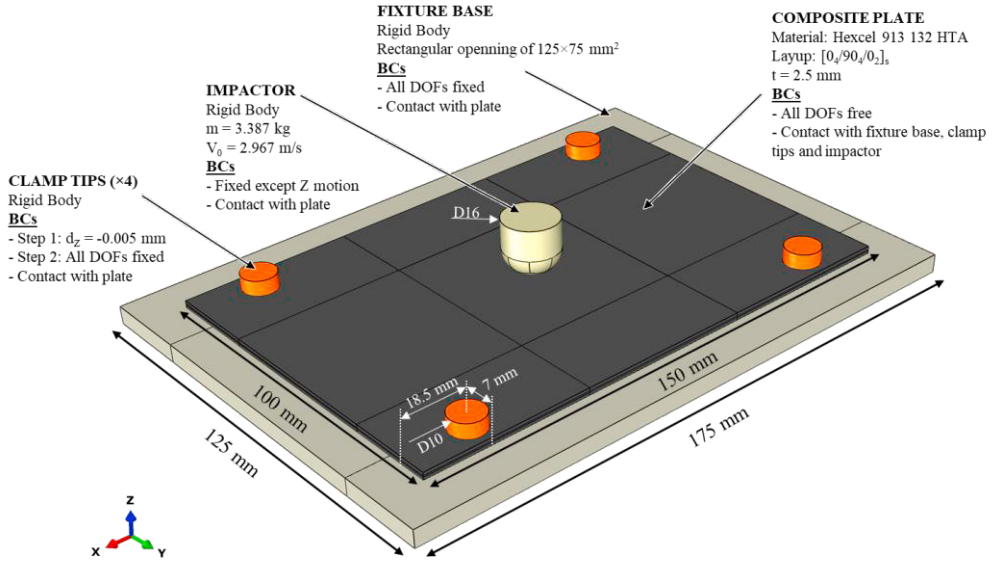

Fig. 2. Geometry and boundary conditions of the virtual impact test setup.

4. Results

Finite element analysis of the 15 J - impact experiment on the $[0_4/90_4/0_2]_s$ CFRP plate specimen was performed in a high performance workstation using 30 central processing unit. Variable mass scaling technique is used to prevent decrease of the stable time increment under a predefined value. The analysis ran for 3 days until it was terminated 5 milliseconds after the initial contact due to the rebound of the impactor. In this section, results obtained from the finite element analysis are presented.

Fig. 3 shows the matrix damage distribution under the impact zone at different contact times, t. One quarter of the plate is removed for clear visualization of the damage states in both y-z and x-z planes under the impactor. The sequence of the damage process can be summarized as follows,

- The first frame is taken at $t_i = 0$ at which the initial contact between the impactor and the beam happens.
- At $t_i = 0.06$ ms, initial matrix crack forms in the bottom layers where the maximum elongation due to bending occurs. This form of the failure is similar to the one observed in the line impact experiments of $[90/0]_s$ beams. Although the stacking sequence of the plate is $[0_4/90_4/0_2]_s$ in the plate coordinate system, matrix cracking of the bottom plies is expected initial failure mode independent from the stacking sequence due to the spherical shape of the impactor, the plate geometry and the boundary conditions.
- At $t_i = 0.13$ ms, the initial matrix crack propagates in the bottom group of 0° plies. A damaged region starts to form in the lowermost ply of the laminate. Some shear and bending cracks and delaminations are also observed through the thickness of the plate.
- At $t_i = 0.30$ ms, the initial matrix crack propagates in the bottom ply along the principal axis of the plate. Delamination initiation is completed at all 0/90 interface at this instant. Additionally, matrix damage occurs in the top 0° plies around the boundary of the contact between the impactor and the plate.
- At $t_i = 0.40$ ms, further matrix crack propagation is observed in the bottom ply along the principal axis of the plate.

- At t_i = 1.00 ms, matrix damage in the bottom ply expands out from the impact zone. A significant increase in sizes of the existent delaminations in two interfaces of the beam are observed in this frame.
- At t_i = 2.00 ms, the existent matrix damage and delaminations grows outwards from the center of the plate. Multiple vertical matrix cracks occur in the top 0° plies. It can be observed that delamination growth occurs mainly in the orientation of the bottom layer.
- The last frame shows the distribution of the complicated matrix damage state inside the laminate when the impactor reaches the maximum displacement at t_i = 4.10 ms.

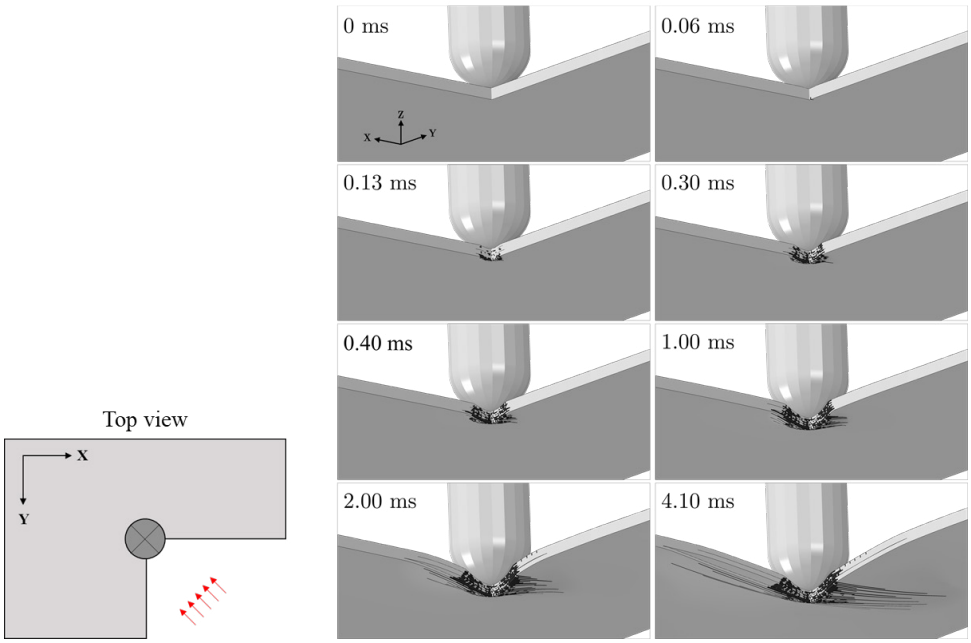

Fig. 3. Through-the-thickness views matrix damage distribution under the impact zone at different contact times (Images are taken with multiple cut planes: x-z and y-z).

Fig. 4a shows the delamination damage at the end of the analysis (t_i = 5.00 ms) at each four 0/90 interfaces starting from the uppermost. The pictures encircle the 100 × 100 mm^2 central region of the plate. This result show that delaminations propagate forming a peanut shape with a major axis in the same orientation as of the lower adjacent ply in accordance with the experiments presented in the literature (Abrate, 1991). Fig. 4b compares the projected delaminations obtained in the experiment and the simulation. It should be noted that the experiment is conducted with the identical conditions for comparison purposes. Although overall projected delaminated area is larger in case of simulations, a good agreement was obtained in terms of the extent of the delamination in the direction of plate length.

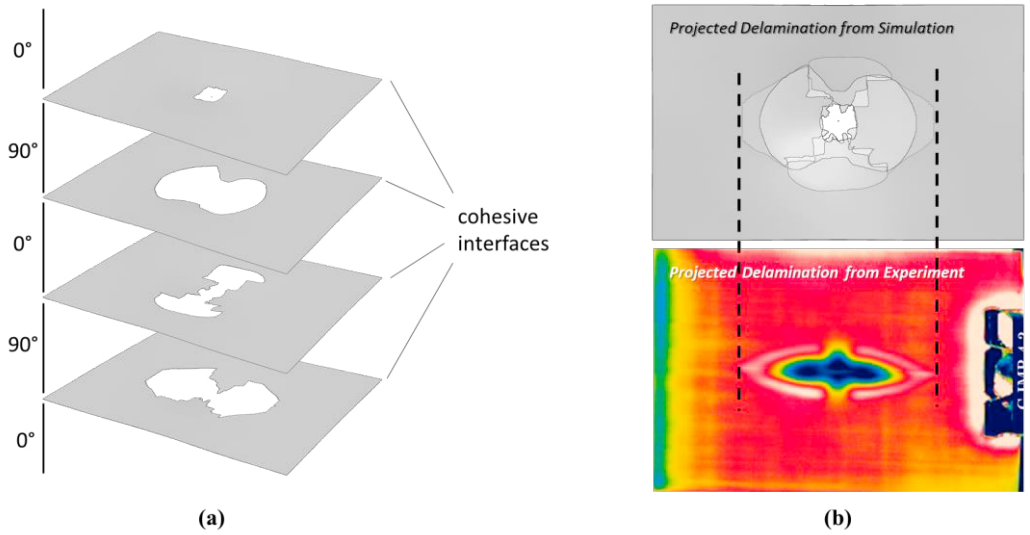

Fig. 4. (a) Delamination damage at 0/90 interfaces of the laminate at the end of the simulation and (b) comparison of the projected delaminations obtained in the simulation and the experiment.

5. Conclusions

In this study, a virtual impact test setup was modeled and finite element analysis of the 15 J – impact event on the $[0_4/90_4/0_4]_s$ CFRP plate specimen was conducted in ABAQUS/Explicit. The material model accounting matrix and fiber failure modes of the fiber reinforced composites was developed and implemented into the model via a user-written subroutine VUMAT. Delamination damage in the plate was simulated by inserting cohesive elements at the interfaces of plies with different orientations.

The results of the present analysis show that the initial failure mechanism in the 3-D low-velocity impact event is the matrix cracking in the lowermost plies independent from the stacking sequence of the laminate. Although matrix cracking does not lead to a considerable drop in the impact load, it should be taken into account in the analyses since it promotes formation of delamination which is one of the most energy dissipative failure modes of composites. It is also observed that delaminated regions expand in the same direction as of the fibers of the lower adjacent layer in accordance with the bending stiffness mismatching concept.

Acknowledgements

This work is supported by Turkish Aerospace – Rotary Wing Technology Center under contract DKTM/2015/05. The authors of the paper would like to thank METU Center for Wind Energy for the use of their facilities.

References

Abrate, S., 1991. Impact on laminated composite materials. Appl.Mech. Rev., 44(4), 155-190.

ASTM International, 2012. Standard D7136 - standard test method for measuring the damage resistance of a fiber reinforced polymer matrix composite to a drop weight impact event. http://dx.doi.org/10.1520/D7136.

Benzeggagh M.L., Kenane M., 1996. Measurement of mixed-mode delamination fracture toughness of unidirectional glass/epoxy composites with mixed-mode bending apparatus. Composite Science and Technology; 56:439–49.

González, E. V., Maimí, P., Camanho, P. P., Turon, A., and Mayugo, J. A., 2012. Simulation of drop-weight impact and compression after impact tests on composite laminates. Composite Structures, Vol. 94, (11), pp. 3364-3378.

Hashin, Z., 1980. Failure criteria for unidirectional fiber composites. Journal of applied mechanics, Vol. 47, (2), pp. 329-334.

Joshi, S.P. and Sun, C.T., 1985. Impact induced fracture in a laminated composite. J. Compos. Muter., 19, 51-66.

Lopes, C. S., Camanho, P. P., Gürdal, Z., Maimí, P., and González, E. V., 2009. Low-velocity impact damage on dispersed stacking sequence laminates. Part II: Numerical simulations. Composites Science and Technology, Vol. 69, (7-8), pp. 937-947.

Lopes, C. S., Sádaba, S., González, C., Llorca, J., and Camanho, P. P., 2016. Physically-sound simulation of low-velocity impact on fiber-reinforced laminates. International Journal of Impact Engineering, Vol. 92, pp. 3-17.

Simulia, 2012. ABAQUS 6.12-2 - analysis user manual. Providence (RI, USA).

Soto, A., González, E. V., Maimí, P., de la Escalera, F. M., de Aja, J. S., and Alvarez, E., 2018. Low velocity impact and compression after impact simulation of thin ply laminates. Composites Part A: Applied Science and Manufacturing, Vol. 109, pp. 413-427.

Topac, O. T., Gozluklu, B., Gurses, E., and Coker, D., 2017. Experimental and computational study of the damage process in CFRP composite beams under low-velocity impact. Composites Part A: Applied Science and Manufacturing, Vol. 92, pp. 167-182.